Dual-beam Holographic Deflection Measurement

A holographic method is established to measure full-field deflection with variable sensitivity

by J.A. Gilbert and J.W. Herrick

ABSTRACT—Deflection is recorded at different sensitivities over a limited portion of the holographic range by introducing equal but opposite phase changes into the holograms created by a dual-beam illumination. The technique does not require a partially reflecting mirror, patterns can be optically filtered for better fringe contrast and in-plane displacement can be recorded without making any modifications in the experimental setup. Results obtained from two- and three-dimensional surfaces agree well with theory and verify analytical arguments presented throughout the paper.

List of Symbols

$\mathbf{d}$ = displacement vector
d_i = inner diameter of pipe
d_o = outer diameter of pipe
$\hat{\mathbf{e}}_i$ = unit vector in direction of propagation
n_i = fringe order number
r, θ, Z = polar coordinates
C = center of rotation
D = distance between model and photographic plate
E = elastic modulus
L = length of pipe
M_t = applied torque
P = object point
R = radius of disk
U, V, W = scalar components of displacement
X, Y, Z = cartesian coordinates
Z_c = distance between photographic plate and rotation center
α = sensitivity angle
β = angle of rotation
δ = fringe spacing
θ_R = reference-beam angle
λ = wavelength
ν = Poisson's ratio
ξ = radial coordinate
ϕ_p = induced phase change

Introduction

Full-field holographic deflection patterns are usually recorded by illuminating and viewing a specimen along the same direction with the aid of a partially reflecting mirror. When holograms of the undeformed and deformed specimen are superimposed, a holographic interferogram is recorded in which fringes become apparent upon reconstruction. Points lying on the same fringe have experienced equal changes in optical path while points on two adjacent fringes have moved through a distance of one-half a wavelength relative to one another in the direction of illumination/observation.

This paper presents a holographic method which records deflection with different sensitivities over a limited portion of the holographic range. The technique does not require a partially reflecting mirror, patterns can be optically filtered for better fringe contrast and in-plane displacement can be recorded without making any modifications in the experimental setup.

Analysis

As shown in Fig. 1, a model is illuminated with two beams contained in the X,Z plane. The two beams, characterized by unit vectors $\hat{\mathbf{e}}_1$ and $\hat{\mathbf{e}}_2$, make equal angles α with respect to the viewing direction given by the unit

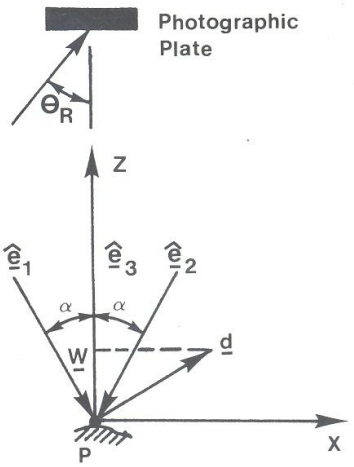

Fig. 1—Displacement analysis of a point

J.A. Gilbert (SESA Member) is Assistant Professor, University of Wisconsin-Milwaukee, Milwaukee, WI 53201. J.W. Herrick is Development Engineer, General Electric Medical Systems Division, Milwaukee, WI 53201.

Paper was presented at Fourth SESA International Congress on Experimental Mechanics held in Boston, MA on May 25-30, 1980.

Original manuscript submitted: June 17, 1980. Authors notified of acceptance: December 19, 1980. Final version received: February 5, 1981.

vector $\hat{\mathbf{e}}_3$. A photographic plate, situated along the observation direction, is used to capture these wavefronts with a reference beam at an angle θ_R with respect to the plate normal.

When points on the object surface are displaced through a vector displacement **d** between photographic recordings, two holograms are generated which display interference fringes given by[1]

$$(\hat{\mathbf{e}}_1 - \hat{\mathbf{e}}_3)\cdot\mathbf{d} = n_1\lambda \quad (1)$$

and

$$(\hat{\mathbf{e}}_2 - \hat{\mathbf{e}}_3)\cdot\mathbf{d} = n_2\lambda \quad (2)$$

where n_1 and n_2 are fringe order numbers and λ is the wavelength of the laser used during the recordings. Displacement is projected along sensitivity vectors $(\hat{\mathbf{e}}_1 - \hat{\mathbf{e}}_3)$ and $(\hat{\mathbf{e}}_2 - \hat{\mathbf{e}}_3)$ in eqs (1) and (2), respectively. The two sets of holographic fringes are referred to as component patterns.

The component patterns created by a dual-beam illumination have been superimposed to form a moiré pattern which corresponds to the difference in phase between them. Displacement is projected normal to the angle bisector of the illuminating beams, parallel to the plane formed by their respective propagation vectors. In general, the moiré is enhanced by densifying the component patterns either by rotating the object,[2] the photographic plate,[3] the illuminating beams[4] or a sandwich hologram.[5] All of these procedures are used to introduce common phase changes into each of the component patterns.

Phase changes of equal magnitude and opposite sign have been introduced into each component pattern to project displacement along the angle bisector of the dual-beam illumination. This was accomplished by rotating the illumination in opposite directions between exposures.[4] The latter is not always feasible; for example, when fiber optics are used to measure deformation in a remote region of a structure.[6] In this case, the illumination is difficult to adjust once the fiber optics have been inserted into the system.

This paper describes an alternate method which records displacement along the angle bisector of a dual-beam illumination. Sensitivity can be varied over a limited portion of the holographic range. As shown in Fig. 1, the test surface is observed along the angle bisector of a dual-beam illumination. Equal but opposite phase changes are then introduced into the component patterns by moving the photographic plate between exposures.

Moving the photographic plate between exposures causes a visible interference pattern.[3] When the plate is rotated around any axis parallel to the plate, straight-line fringes with fringe spacing,

$$\delta = \frac{\lambda}{\beta(1 - \cos\theta_R)} \quad (3)$$

localize in space at a distance,

$$D = \frac{Z_C}{1 - \cos\theta_R} \quad (4)$$

from the plate. In eqs (3) and (4), β is the rotation initiated to the plate measured in radians, θ_R is the angle measured to a collimated reference wavefront from the plate normal, and Z_C is the distance from the hologram to the rotation center. Once θ_R is established, Z_C is chosen in accordance with eq (4) to localize the interference pattern very close to the object surface. The fringe pattern which results from plate motion is called an initial pattern.

Equation (3) also holds true for image plane holographic recordings where D is nearly zero. In this case, the plate is rotated about an axis passing through the plane of the plate for proper localization.

Consider a hologram recorded with the configuration shown in Fig. 1. The plate is mounted so that rotation can be carried out around an axis parallel to the plane of the plate which passes through a rotation center whose position can be varied along $\hat{\mathbf{e}}_3$.

If the plate is rotated between exposures, both the reference and object wavefronts are modulated and an additional phase change ϕ_p is experienced by each model point. In general, ϕ_p is a function of all three displacement components U, V, W. This phase change is equivalent to a pure rigid body rotation of the model around a rotation axis passing through a point which lies at a distance D, measured along Z, normal to the plate.[7] When one component pattern, say that given by eq (2), is recorded with an equal but opposite rotation to that used to modulate the pattern given by eq (1), the expressions for the new component patterns become,

$$(\hat{\mathbf{e}}_1 - \hat{\mathbf{e}}_3)\cdot\mathbf{d} + \phi_p(U, V, W) = n_3\lambda \quad (5)$$

and

$$(\hat{\mathbf{e}}_2 - \hat{\mathbf{e}}_3)\cdot\mathbf{d} - \phi_p(U, V, W) = n_4\lambda \quad (6)$$

Equations (5) and (6) can be formulated in terms of U, V, W and the sensitivity angle α as,

$$U\sin\alpha - (1 + \cos\alpha)W + \phi_p(U, V, W) = n_3\lambda \quad (7)$$

and

$$-U\sin\alpha - (1 + \cos\alpha)W - \phi_p(U, V, W) = n_4\lambda \quad (8)$$

When these patterns are viewed simultaneously along $\hat{\mathbf{e}}_3$, they optically superimpose to form a moiré. The

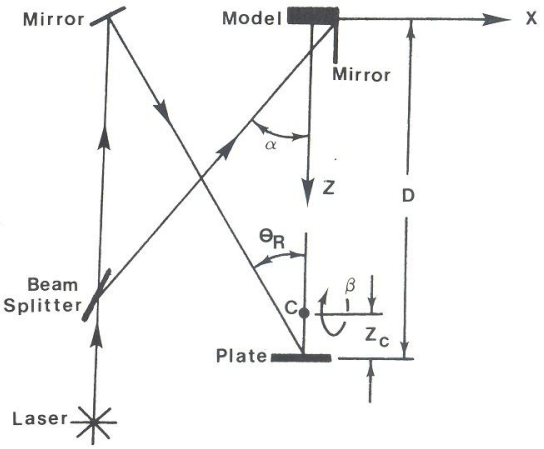

Fig. 2—Experimental setup

latter can be expressed parametrically as either the sum or difference of eqs (7) and (8). The angular orientation of the component patterns determines which family of moiré is predominate.[8]

Under some circumstances, difficulties may arise in the interpretation of the moiré-fringe pattern. The latter may have a tendency to fade out in areas where there are large variations of fringe spacing in the component patterns. In more severe cases, the angular orientation of the component patterns causes their superposition to form one moiré family, say the sum, which abruptly changes to form the other family; namely, the difference.

The induced phase change caused by plate rotation has a direct bearing on both the fringe spacing and orientation in each component pattern. Ordinarily their difference is apparent; however, when the phase change due to plate rotation exceeds that caused by model deformation, the moiré pattern corresponding to the sum becomes predominate. Adding eqs (7) and (8) one obtains,

$$2(1 + \cos \alpha) W = -(n_3 + n_4)\lambda = n_w \lambda \qquad (9)$$

where n_w is the moiré-fringe order number of the sum.

Equation (9) represents the projection of $\mathbf{d}$ along $\hat{\mathbf{e}}_3$ and is commonly referred to as the deflection when dealing with a flat surface in the X,Y plane. Sensitivity can be varied by changing α. The lower bound, corresponding to $\alpha = 90$ deg, can only be achieved for flat surfaces, since this condition describes grazing incidence. Each fringe in the moiré pattern is a multiple of $\lambda/2$, which is analogous to the result predicted for full-field holographic deflection measurement carried out by illuminating and viewing a specimen along the same direction with the aid of a partially reflecting mirror. The upper bound corresponds to $\alpha = 0$ deg. In this case, points on adjacent fringes move through $\lambda/4$ with respect to one another.

The following section documents experiments carried out on two- and three-dimensional surfaces with the proposed technique. Each test is performed with illuminations at different sensitivity angles to fully verify eq (9).

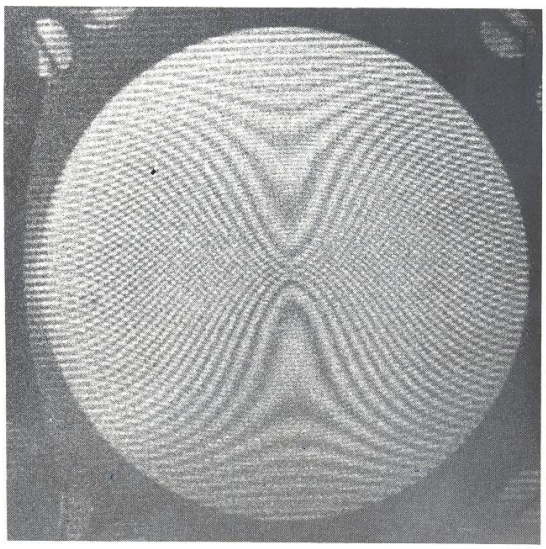

Fig. 3—Deflection pattern for a centrally loaded circularly clamped plate with a center deflection of 7.62×10^{-4} cm, recorded with $\beta = 11.25$ arc minutes

Experimental

The method outlined above is first applied to a two-dimensional surface. A centrally loaded circularly clamped plate is constructed by sandwiching a 12.7-cm-diam, 0.32-cm-thick Plexiglas disk between a retaining plate and a steel frame. The inner lip of the retaining plate creates an effective 7.62-cm-diam fixed-support condition. The test surface is painted flat white; deflection is initiated at the center of the plate with a micrometer located behind the model surface. A 0.79-cm-diam steel ball provides the contact point.

Displacement along the line of sight is recorded with the experimental setup shown in Fig. 2. The test surface is located in the XY plane. A front-surface mirror, positioned parallel to Z, allows two collimated beams to be constructed from a single source so that experiments can be carried out using a lower powered laser than would ordinarily be necessary if two separate object beams were used to illuminate the specimen. The illuminations, which are contained in the X,Z plane, make equal angles, $\alpha = 45$ deg, with respect to the Z axis. A shutter system is also included in the object-beam wavefront to allow the test surface to be separately illuminated with either beam.

The photographic plate is positioned so that rotation can be carried out around an axis parallel to X, passing through C. The parameters θ_R, Z_C and D are chosen in accordance with eq (4) to localize the initial pattern on the object surface as $\theta_R = 30$ deg, $Z_C = 5.44$ cm and $D = 40.64$ cm, respectively.

An initial exposure is taken of the unloaded model with both beams illuminating the model. The load is applied to the specimen and the photographic plate is rotated through a counterclockwise angle β. This modified state is recorded with illumination from the right. The plate is rotated through 2β clockwise and a third exposure is taken with illumination from the left. The plate is then developed and reconstructed.

Figure 3 shows the superposition of the component patterns when the center of the centrally loaded circularly clamped plate moves along Z, through a deflection of 7.62×10^{-4} cm. The pattern is recorded with an induced phase change corresponding to $\beta = 11.25$ arc minutes. The sum of the component patterns is visible only in those areas where the ratio of the induced phase to that caused by model deformation is sufficient to produce the corresponding moiré. This occurs close to the fixed boundary where the deformation is small. Figure 4, on the other hand, corresponds to a center deflection of 1.40×10^{-4} cm, recorded with a plate rotation of $\beta = 15$ arc minutes. In this case, the moiré is visible over the entire test surface. The ratio of the induced phase change to that caused by deformation in Fig. 4 is 7.3 times that in Fig. 3.

Theoretically, the equal but opposite rotations given to the photographic plate between exposures result in two identical fringe patterns. The manner in which they superimpose with the deformation, however, depends on the direction of rotation. Any difference in the orientation and/or the spacing of the fringes in the initial pattern

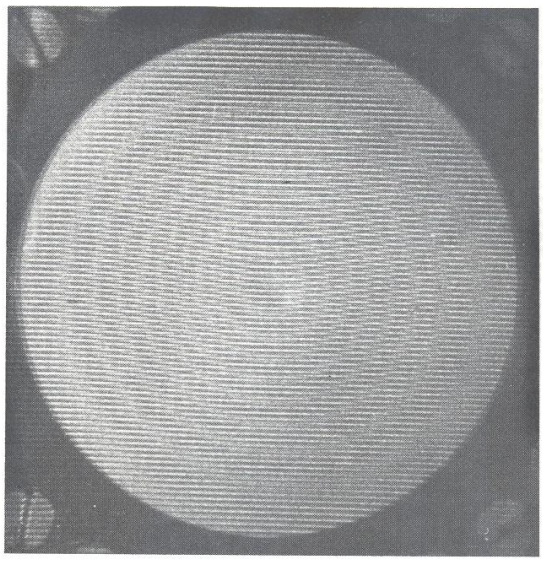

Fig. 4—Deflection pattern for a centrally loaded circularly clamped plate with a center deflection of 1.40×10^{-4} cm, recorded with $\beta = 15$ arc minutes

induced in each of the component patterns produces a mismatch when they are superimposed. This will shift the displacement pattern. A careful examination of the fringe pattern shown in Fig. 4 reveals that, contrary to theory, the displacement fringes are not concentric. The filtered pattern is shown in Fig. 5 in an effort to explore this apparent error.

Fig. 5—Filtered pattern of the deflection pattern for a centrally loaded circularly clamped plate

Recall that the induced phase change was introduced by rotating the photographic plate about a horizontal axis; the latter corresponds to an axis parallel to X, passing through C on Fig. 2. Theoretically, this results in parallel, horizontal fringes in the absence of model deformation.[3] Introducing a different number of fringes into each component pattern by opposite but unequal rotations of the photographic plate would cause horizontal mismatch fringes. If this fringe pattern were superimposed with that due to the deformation of the centrally loaded circularly clamped plate, the moiré would be shifted in the vertical direction. A horizontal shift would occur for a rotational mismatch.

Assuming that the centrally loaded circularly clamped plate has been properly constrained, the mismatch has shifted the displacement pattern in a direction at 45 deg measured clockwise with respect to the horizontal. This indicates that there was a difference in both spacing and orientation of the fringes introduced into each component pattern.

Figure 6 shows the displacement plotted parallel and perpendicular to the shift. The mismatch does not effect displacement measured perpendicular to the shift; consequently, the mismatch can be determined for displacement measured along the shift by subtracting the fringe order numbers in the two experimental plots. The mismatch is included in the figure. The displacement along the shift can now be corrected by subtracting off the displacement due to the mismatch. The comparison of these results with theory[9] indicates that the method is accurate provided that equal but opposite phase changes are introduced into the component patterns.

A thin-walled, PVC pipe is used as a three-dimensional test surface. As shown in Fig. 7, the pipe is rigidly fixed at end $X/L = 0$ and a torque, M_T, is applied at $X/L = 1.0$, to produce a state of pure torsion. Geometrical parameters, material properties and coordinate axes are included in the figure.

The setup shown in Fig. 2, and the procedure outlined for the centrally loaded, circularly clamped plate are used to record the displacement pattern for the pipe; however, in this test, illuminations are contained in the Y, Z plane, make angles of 30 deg with respect to the Z axis and illuminate the region of interest from $0.4 \leq X/L \leq 0.6$. Figure 8 shows the component patterns and their moiré recorded with $\beta = 11.25$ arc minutes. No information is obtained for $|2\,Y/d_0| \geq 0.43$, where d_0 is the outer diameter of the pipe. In this region, only a single beam illuminates the pipe and no moiré is formed. The displacement along Z is given by[10]

$$W = \frac{32 d_0 M_T (1+\nu)}{\pi [d_0^4 - d_i^4] E} (X \cos\theta) \qquad (10)$$

where E, ν and d_i are the Young's modulus, Poisson's ratio and the inner diameter of the pipe, respectively.

Equating eqs (9) and (10) and solving for the fringe order number,

$$n_w = \frac{-64 d_0 M_T (1+\nu)(1+\cos\alpha)}{\lambda\pi [d_0^4 - d_i^4] E} (X \cos\theta) \qquad (11)$$

Using $\lambda = 5145 \times 10^{-8}$ cm, $\alpha = 30$ deg and the information included in Fig. 7, n_w is plotted along $X/L = 0.5$ and compared to the experimental result obtained from

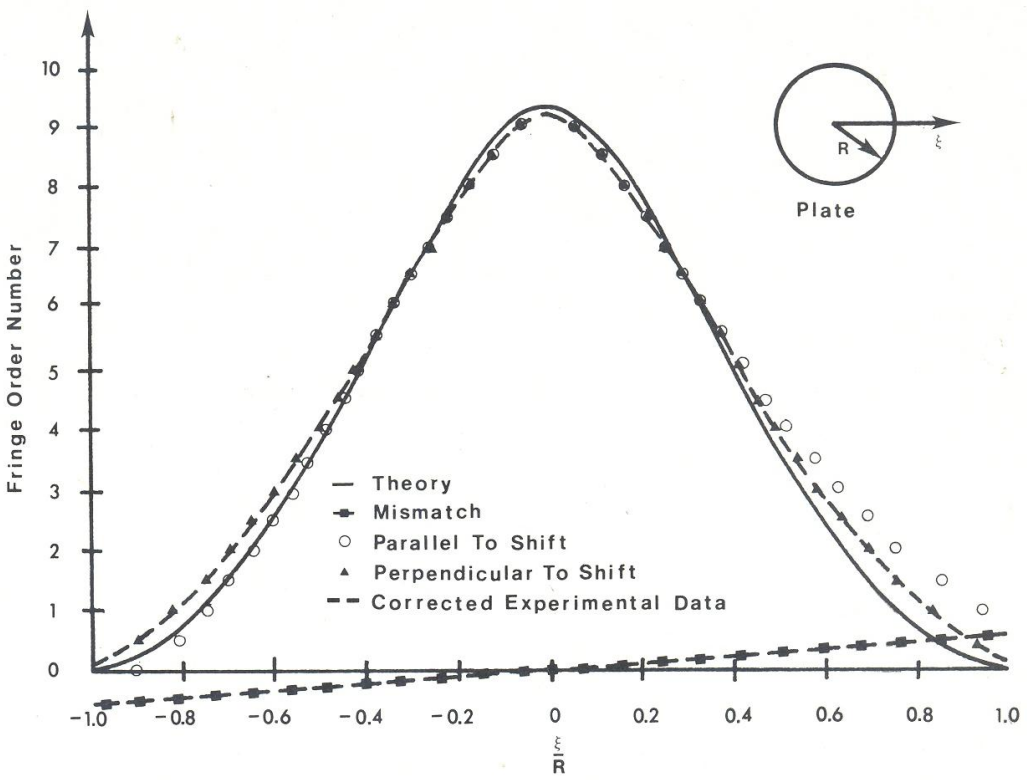

Fig. 6—Displacement, mismatch and theoretical curves for a centrally loaded circularly clamped plate

Fig. 8. This comparison is shown in Fig. 9.

Discussion and Conclusion

Equation (9) has been verified for two- and three-dimensional surfaces; two tests were performed with illuminations at different sensitivity angles.

In each of the experiments used to demonstrate the method, the collimated illuminations given by $\hat{e}_1$ and $\hat{e}_2$

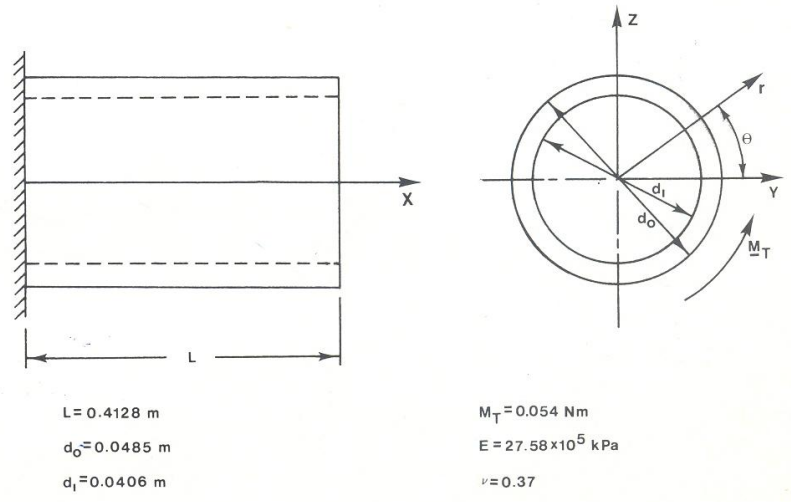

Fig. 7—A pipe subjected to pure torsion

are common over the full-field; however, there is a small change in $\hat{e}_3$ for each model point since one is observing the model from a finite distance. This results in a slight error, since the sensitivity vectors along which displacement is projected are not all parallel to the line of sight. This error can be minimized by making D larger; or, can be eliminated by using an image-plane technique with telecentric viewing.[11] Even with this inherent error, results indicate that the method is accurate and that the technique can be applied to both flat and curved surfaces.

It is impossible to predict the lower bound on induced rotation necessary to produce a visible moiré without knowing the spacing and orientation of the displacement fringes due to actual deformation in each component pattern. A general guideline for practical implementation of the technique, however, is to make the phase change caused by the motion of the photographic plate as large as possible, compared to that due to model deformation. This criterion is best, provided that plate motion can be carefully controlled to avoid mismatch. On the other hand, a known mismatch could be introduced to densify the moiré pattern to facilitate strain analysis. It would be necessary to subtract the induced strain due to the mismatch from derivatives taken from the displacement pattern. This technique is currently under investigation.

One major advantage of the method developed herein is that displacement can also be measured normal to the line of sight without making any modifications in the setup shown in Fig. 2. This procedure is described in detail in Ref. 3.

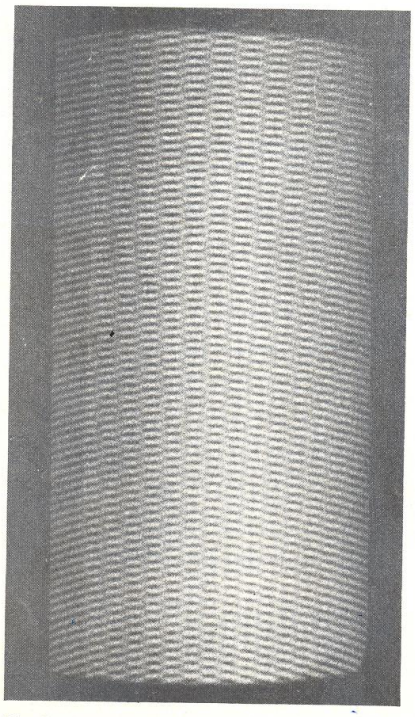

Fig. 8—Deflection pattern for a pipe subjected to pure torsion

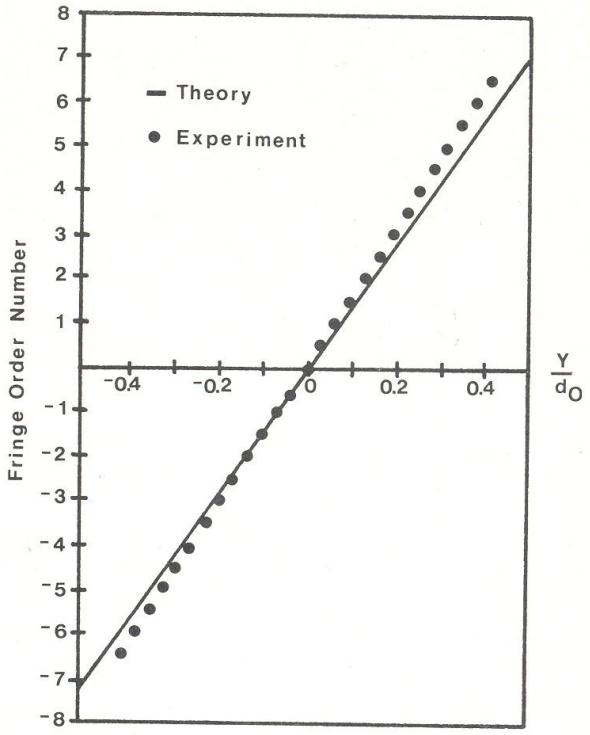

Fig. 9—Theoretical and experimental fringe orders for a pipe subjected to pure torsion along $\frac{X}{L} = 0.5$

References

1. Sollid, J.E., "Holographic Interferometry Applied to Measurements of Small Static Displacements of Diffusely Reflecting Surfaces," Appl. Opt., **8** (8), 1587-1595 (1969).

2. Hung, Y.Y. and Taylor, C.E., "Measurement of Surface Displacements Normal to the Line of Sight by Holo-moiré Interferometry," J. Appl. Mech., **42** (1), 1-4 (1975).

3. Sciammarella, C.A. and Gilbert, J.A., "A Holographic-moiré Technique to Obtain Separate Patterns for Components of Displacement," EXPERIMENTAL MECHANICS, **16** (6), 215-220 (1976).

4. Beranek, W.J. and Bruinsma, A.J.A., "A Geometrical Approach to Holographic Interferometry," SESA Spring Meeting, San Francisco (May 1979), Paper No. R79-149.

5. Abramson, N., "Sandwich Holography: an Analogue Method for the Evaluation of Holographic Fringes," The Engineering Uses of Coherent Optics, Cambridge Univ. Press, Glasgow (1975).

6. Gilbert, J.A. and Herrick, J.W., "Holographic Displacement Analysis with Multimode-fiber Optics," EXPERIMENTAL MECHANICS, **21** (8), 315-320 (1981).

7. Chawla, S.K. and Sciammarella, C.A., "Localization of Interference Fringes Produced by Rotation of Plate in Focused-image Holography," SESA Spring Meeting, San Francisco (May 1979), Paper No. R79-167.

8. Durelli, A.J. and Parks, V.J., Moiré Analysis of Strain, Prentice Hall, NJ (1970).

9. Roark, R.J. and Young, W.C., Formulas for Stress and Strain, 5th Edition, McGraw-Hill (1976).

10. Timoshenko, S., Strength of Materials, D. Van Nostrand Company (1940).

11. Gilbert, J.A. and Exner, G.A., "Holographic Displacement Analysis using Image-plane Techniques," EXPERIMENTAL MECHANICS, **18** (10), 382-388 (1978).